

FT-ICR MS characterization of bio-binders for road pavement from HTL of microalgae residues

Christophe Geantet, Dorothée Laurenti, Nolven Guilhaume, Chantal Lorentz, Ilef Borghol, Bruno Bujoli, Emmanuel Chailleux, Ruben Checa, Sébastien Schramm, Vincent Carré, et al.

▶ **To cite this version:**

Christophe Geantet, Dorothée Laurenti, Nolven Guilhaume, Chantal Lorentz, Ilef Borghol, et al.. FT-ICR MS characterization of bio-binders for road pavement from HTL of microalgae residues. Journal of Environmental Chemical Engineering, 2022, 10 (3), pp.107361. 10.1016/j.jece.2022.107361 . hal-03805906

HAL Id: hal-03805906
https://hal.science/hal-03805906

Submitted on 7 Oct 2022

HAL is a multi-disciplinary open access archive for the deposit and dissemination of scientific research documents, whether they are published or not. The documents may come from teaching and research institutions in France or abroad, or from public or private research centers.

L'archive ouverte pluridisciplinaire **HAL**, est destinée au dépôt et à la diffusion de documents scientifiques de niveau recherche, publiés ou non, émanant des établissements d'enseignement et de recherche français ou étrangers, des laboratoires publics ou privés.

FT-ICR MS characterization of bio-binders for road pavement from HTL of microalgae residues

Christophe Geantet,[1*] Dorothée Laurenti,[1] Nolven Guilhaume,[1] Chantal Lorentz,[1] Ilef Borghol,[2,3] Bruno Bujoli,[2] Emmanuel Chailleux,[3] Ruben Checa,[1] Sébastien Schramm,[4,5] Vincent Carré,[4,5] Frédéric Aubriet[4,5] and Clémence Queffélec[3*]

1. Univ Lyon, Université Claude Bernard Lyon 1, CNRS, IRCELYON UMR 5256, F-69626 Villeurbanne Cedex, France

2. Université de Nantes, CNRS, CEISAM, UMR 6230, F-44000 Nantes, France

3. Université Gustave Eiffel, Campus de Nantes, Allée des ponts et chaussées - CS 5004, 44344 Bouguenais Cedex, France

4. Université de Lorraine, LCP-A2MC, F-57000 Metz, France

5. Réseau National de Spectrométrie de Masse FT-ICR à très haut champ (FR 3624), Université de Lorraine, F-57000 Metz, France

Abstract

Hydrothermal liquefaction (HTL) of microalgae-derived feedstocks into a bio-binder was investigated in the absence or presence of a catalyst. The resulting products of HTL of Scenedesmus species (sp.) residues present rheological properties close to those observed with a petroleum bitumen. The chemical composition of the biobinder was analysed by two-dimensional gas chromatography (GCxGC-MS), by gel permeation chromatography (GPC), and negative and positive-ion laser desorption/ionization FT-ICR MS to provide a complementary analysis of the biobinder and understanding of the role of catalysts. A detailed description of the heavy nitrogen compounds contained in the biobitumen is given.

Key-words: Hydrothermal liquefaction, microalgae, Scenedesmus residues, FT-ICR MS, Biobinder, rheology, ceria

1. Introduction

One of the main challenges nowadays is the use of renewable feedstocks in place of fossil resources. This includes petroleum bitumen (natural origin or derived from the distillation of petroleum). Petroleum bitumen is a sticky viscoelastic material mostly used to bind aggregate in pavement mixture. Thus, in order to promote a transition to a low-carbon economy, the search for renewable resources for road materials is therefore essential while not competing with more essential uses of biomass, such as human nutrition or energy. In this context, microalgae have appeared as an interesting option.

Currently microalgae are cultivated for various applications such as cosmetic and nutritional supplements. Extraction of useful compounds give residues which are currently not valorized and could be used to produce biobinders. Thus, in this work, we focused on Scenedesmus microalgae residues. *Scenedesmus* sp. is a promising microalgae for biodiesel production due to its high growth rate in summer[1] and to its high lipid content. In this work, *Scenedesmus* sp. microalgae were grown by the Alpha-Biotech company (Asserac, France) which valorizes the major part of the water-soluble proteins recovered by centrifugation.

Hydrothermal liquefaction (HTL) is considered as one of the most promising process to transform wet biomass, and especially wet microalgae, into bio-oils and high added value products, under high temperature (250–350 °C) and pressure (5–15 MPa) conditions.[2–4] In former studies, we have reported that biobinders with properties similar to petroleum bitumen could be obtained through the transformation of microalgae residues by HTL at 260 °C.[5,6] Recently, a lot of studies have been dedicated to the use of a catalyst during HTL conversion

because it may affect the composition of the hydrophobic phase and provide new interesting properties.[7–13]

We have previously demonstrated that the HTL of *Scenedesmus* sp. residues at 260 °C led to a biobinder with rheological properties similar to a petroleum bitumen.[5,14] We thus decided to investigate whether the addition of a catalyst during HTL might influence the rheological properties of the resulting biobinder. Usually, catalysts are used to lower the high acidic level and high heteroatoms content (e.g. O and N) and thus improve the calorific value of the biocrude obtained after HTL, to allow its use as a green biofuel. In contrast, our objective was to modify the viscosity and rheology of the biocrude, by increasing the carbon chain size and removing part of the heteroatoms. Thus, $Ce(NO_3)_2.6H_2O$ was selected as a catalyst because it can catalyse the ketonization reaction[15,16] that leads to longer chains ketones or hydrocarbons during HTL. One challenge while performing HTL is to characterize the high molecular weight components in the hydrophobic fraction in order to optimize the biomass transformation. In this paper, different chemical characterization techniques were applied to analyse the hydrophobic fraction in a wide molecular weight range. In that regard, two-dimensional gas chromatography coupled with mass spectrometry (GCxGC-MS) and gel permeation chromatography (GPC) were used to investigate low to medium mass range fractions (160 to 55 000 g/mole eq. PS). Complementarily, FT-ICR MS[17,18] was also used since it is a high-resolution mass spectrometry technique that also allows to determine accurate mass to charge (m/z) ratio of ions and then access to elemental composition and double bond equivalent. This technique has been recently used to analyze really complex mixtures including liquefaction products.[19–31]

This study shows that the whole hydrophobic fraction obtained after HTL of microalgae residues led to a biobitumen with similar rheological properties as petroleum bitumen but which differ significantly in chemical composition, in particular in terms of N-containing compounds.

but which differ significantly in chemical composition, in particular in terms of N-containing compounds.

2. Materials and methods

Materials

Scenedesmus sp. microalgae, for which the major part of water-soluble proteins was removed by centrifugation, were purchased from Alphabiotech, Asserac, France. This biomass, that contains about 80 wt % of water, was frozen for storage, and then freeze-dried for 1 week at -90 °C before use.

HPLC-grade solvents were purchased from Aldrich. Reagents were of analytical grade and were used as received from commercial suppliers unless otherwise indicated.

Microalgae residues analysis

The moisture and ash contents were obtained by measuring the weight loss of a 300 mg sample placed in an oven at 110 °C for 2 h or in a tubular furnace at 900 °C in air for 2 hours, respectively.

Conventional methods from the literature were used to assess the amount of proteins,[32] lipids[33,34] and polysaccharides.[35]

Elementary analysis (CHNS-O)

The C, H, N, O and S elemental content was measured using a Thermo Scientific FLASH 2000 series CHNS/O Analyzer, equipped with a thermal conductivity detector (TCD). The analysis was performed twice for each sample. The C, H, N and S percentages were measured after a flash combustion of the sample, generating a gas mixture composed of N_2, CO_2, H_2O and SO_2, which was eluted through a GC column to be analyzed by the TCD detector. Oxygen was analyzed separately, by catalytic pyrolysis of the sample under He, where CO was produced and quantified.

Hydrothermal Liquefaction (HTL) experiments

The hydrothermal liquefaction of Scenedesmus sp. residues was performed in a 300 mL stainless steel batch reactor (PARR 4566) equipped with a mechanical stirring and heating system composed of an electric oven insulated with a glass wool jacket to reduce the heat losses. The internal pressure was measured through a manometer and the temperature was taken inside the reacting medium, using a thermocouple system connected to the Parr 4842 controller.

Almost all experiments were performed under inert atmosphere (N_2) and following the same protocol: 29.9 g of crushed Scenedesmus sp. residues and 119.6 mL of distilled water were introduced in the reactor (keeping a ratio of 4 mL of water per gram of biomass). Otherwise stated, the reactor was kept at 260 °C for 1 h.

Following the above protocol, catalytic HTL was performed by adding cerium nitrate ($Ce(NO_3)_3.6H_2O$) in the initial load at 1 wt.% of cerium with respect to the dried biomass.

Products recovery

After HTL experiment (1h), the system was left to cool down. The gas phase was flushed and was not analyzed. More details can be found in reference ACS Sust. Chem. Eng. 2015, 3, 583-590 in which the same feedstock was used. When opening the reactor, two distinct phases were obtained, the hydrophobic phase at the bottom of the reactor and the supernatant aqueous phase. The aqueous phase was directly poured from the reactor into a storage flask and the sticky hydrophobic phase remaining in the reactor was recovered with a spatula and the remaining fraction on the walls of the reactor were washed with DM, combined with the hydrophobic fraction and the DCM was evaporated under reduced pressure. Subsequently, the solvent was evaporated under reduced pressure and the hydrophobic fraction was weighted to calculate the bio-oil yield, based on the initial biomass, applying equation (1).

Equation (1) $Yield = (W_{hydroph})/ (W_i) * 100$

When cerium nitrate hexahydrate was employed as a catalyst, the latter was converted *in situ* into cerine (CeO_2). In this case, equation (2) was used to subtract the contribution of the catalyst.

Equation (2) $Yield = (W_{hydroph} - W_{cat})/ (W_i) * 100$

With $W_{hydroph}$ = Weight (g) of the hydrophobic phase

W_{cat} = Weight of cerium nitrate hexahydrate * Molecular weight of cerine / Molecular weight of cerium nitrate hexahydrate (g)

W_i = Weight (g) of initial biomass

FT-IR

ATR-FTIR spectra were obtained in the 600-4000 cm^{-1} range with a Bruker Vector 22 FTIR spectrometer.

Gel permeation chromatography (GPC)

The size exclusion analysis was carried out with an Agilent apparatus (1200 series) equipped with two PL gel porous columns of different pore size (500-50 Å) and a differential refractive index (DRI) detector, using tetrahydrofuran (THF) as the mobile phase. Each sample was diluted at 5 wt % in THF and filtered using a syringe filter with a pore size of 0.45 μm.

The system was calibrated using polystyrene (PS) standards with a molecular weight distribution from 162 to 55 100 g/mol. Therefore, the distribution is not absolute, but relative to the calibration curve (PS equivalent).

Bi-dimensional gas chromatography (GCxGC)

The analysis was carried out with an Agilent 6890 apparatus, using a semi-polar capillary column ZB-35 of 30 m length (35 % phenyl and 65 % dimethylpolysiloxane) as the first column

and a nonpolar capillary column DB-1 of 2 m length (100 % dimethylpolysiloxane) as the second column. Two detectors were used to analyze the samples: a mass spectrometry (q-MS Agilent 5975B) detector, for products identification and qualitative analysis, and a flame ionization detector (FID) for quantitative analysis, where decane was used as a reference internal standard.

Some samples were diluted in THF and others in DCM, in a weight percentage among 5-10 %, and all samples were filtered (0.45 μm) before the injection. The method was carried out with an injection volume of 0,5 μL at 310 °C and a split ratio of 50:1. The scan mass spectra were measured in the range of 33-280 m/z.

FT-ICR MS

The compounds were characterized by FT-ICR MS (IonSpec, Lake Forest, CA) fitted with a 9.4 T shielded superconducting magnet. The biocrude products were investigated by laser desorption/ionization at low laser fluence (LDI). The laser fluence was adjusted to be just above the laser/desorption ionization threshold to avoid fragmentation and recombination phenomena. The excitation wavelength was 355 nm and therefore ionization of aromatic structures especially the heteroaromatic ones was favored as compared to alkenes or saturated oxygenates. As compared to commonly used ESI, this leads to a more sensitive response but mostly specific to aromatic and heteroaromatic compounds as it has been illustrated in the case of humic substances[36] or bio-oils.[37–39] Therefore, comparison from the literature between the two methods is not straightforward. The used acquisition parameters were controlled by the Omega software (Varian). The products obtained from HTL were dissolved in dichloromethane (concentration of 10 mg/mL) and 10 x 1 μL of the solution was deposited on the sample holder. The obtained mass spectra were internally calibrated with a blue pigment (m/z: 471) for negative ions and with a mixture of polyaromatic hydrocarbons (PAH) for positive ions. A peak list of signals with a signal-to-noise (S/N) >4.5 is generated and the Composer software (Sierra

Analytics, Modesto, CA) was used for ion assignment. The interpretation of the obtained data was conducted by using different graphical representations of the obtained features, which reported the average double bond equivalents (DBE) versus the carbon number, the H/C ratio versus the N/C ratio (modified Van Krevelen diagram), and the relative distribution of the ions with respect to the number of heteroatoms.

Rheological analyses

The rheological properties of the bio-binders were measured with a Kinexus pro + rheometer in shear mode, according to the European Standard EN 14770. The water insoluble fractions were loaded, in the melted state at 100 °C, on a plate-plate geometry (with a diameter of 8 mm) with 1 mm gap. Dynamic shear rheometry (DSR) takes measures of phase angles d (°) and of norm of complex modulus (|G*|) at different temperature values, from 80 °C to 0 °C and at various frequencies (from 0.01 Hz to 10 Hz). Measurements were performed in the small strain domain in order to remain in the linear viscoelasticity theory framework.

3. Results and discussion

3.1. Characterization of the *Scenedesmus* sp. residue

Table 1 described the proximate and ultimate algal residue composition. Even though much of water-soluble proteins have been removed, 26% of proteins were still present in the residue as well as 29% of polysaccharides and 17% of fatty acid. The major fatty acids identified were C16:0 (48%), C18:1 (15%), C18:2 (4%) and C18:3 (3%). For comparison, Mandal et al.[40] identified on the whole microalgae Scenedesmus obliquus C16:0 (39%), C18:1 (35.4%), C18:2 (18%) and C18:3 (15%).

Table 1. Chemical composition of the Scenedesmus sp. residues used in this work (measured on freeze dried samples).

Analyses	Scenedesmus sp. residues
Lipids (wt%)	17 ± 0.5
Polysaccharides (wt%)	28.9 ± 0.01
Proteins (wt%)	26 ± 5.4
Ash (wt%)	6.92± 0.5
Moisture (wt%)	7.8 ± 0.1
Elemental analysis	
C	51.32
H	6.94
N	7.11
S	0.44
O	30.28

3.2. Analysis of the HTL and catalytic HTL products

HTL was conducted on *Scenedesmus* sp. residues at 260 °C for 1 h with $Ce(NO_3)_2.6H_2O$ at 1 wt % with respect to the dried biomass. While the catalyst was soluble in water at room temperature, it was fully transformed into cerium oxide (CeO_2) under the HTL experimental conditions.

Yields for HTL reactions were calculated as explained in the Material and methods part. In particular, when cerium nitrate was used, the mass of cerium oxide formed during the reaction was subtracted since it was trapped in the hydrophobic fraction. Indeed, when a blank HTL experiment was run at 260 °C in the presence of only water and cerium nitrate, a white solid was recovered correspond to cerium oxide with ca. 100% yield, as evidenced by its FT-IR spectrum and XRD pattern. This suggests that cerium nitrate is probably the precursor of the active catalyst.[41–43]

The obtained bio-oil yields (Table 2) were close to those previously reported in the literature (for example 35.5% at 300 °C for Scenedesmus abundans[44] or 52% at 350 °C % for Scenedesmus almeriensis[45]).

Table 2. Elemental analysis of the hydrophobic fraction obtained after HTL of the Scenedesmus sp. residues used in this work (using freeze dried samples), in the presence or absence of cerium nitrate.

	Bio-oil yield %	C wt%	H wt %	O wt %	N wt%	S wt%
Without catalyst	39	65.4	8.3	14.02	4.4	0.6
With catalyst	42	66.8	8.7	15.24	4.2	0.4

While similar yields were obtained with or without the presence of cerium nitrate, the aspect (one was viscous and the other one was solid) of the HTL hydrophobic fractions was however much different, suggesting different chemical transformations occurring in the two cases.

The elemental composition of each hydrophobic fraction are summarized in Table 2, while comparison of the H/C and N/C atomic ratio plotted as a function of the O/C atomic ratio is shown in Figure 1.

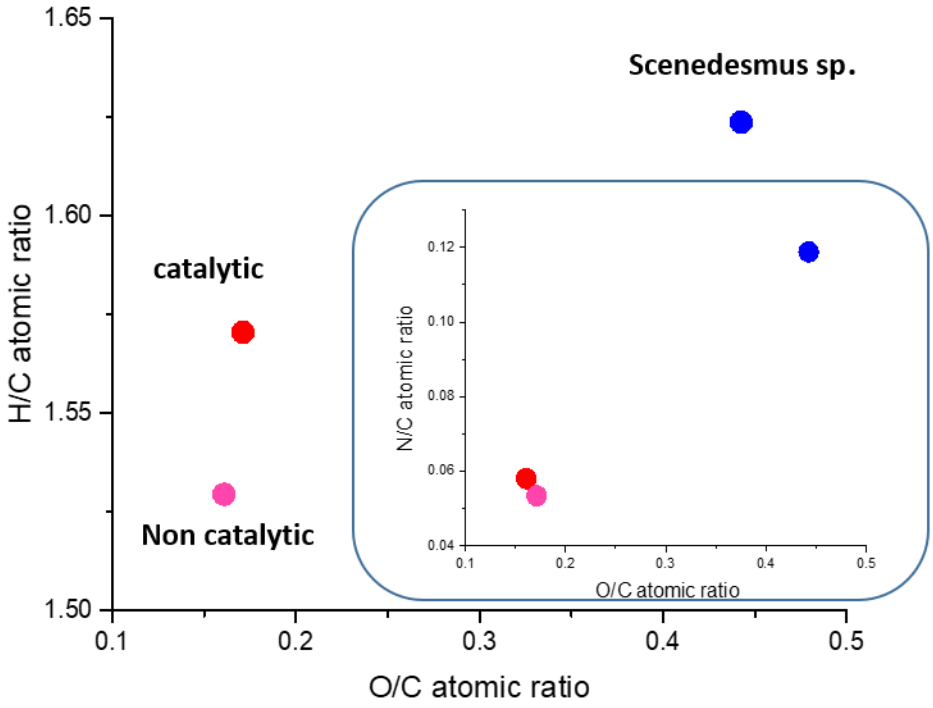


Figure 1. Van Krevelen diagrams of the initial microalgae residues (in blue) and the hydrophobic fractions obtained after HTL (in pink) and catalytic HTL (in red).

Petroleum crude oil is mostly composed of carbon and hydrogen. The composition of the biocrude obtained after HTL still contains heteroatoms (especially N and O) and more organic acids and N-containing compounds than crude oil. However, HTL is known to decrease the oxygen content of the starting feedstock. For both HTL hydrophobic fractions, the O/C, N/C and H/C ratios were clearly lower than in the initial microalgae residues, with a slight difference in the H/ C ratio when cerium nitrate was added, whereas other ratios remained similar. According to Teri at al.[46] the deoxygenation occurring during HTL is always accompanied by the decrease of the H/C ratio. In our case, the HTL of the microalgae residues reduced the O/C atomic by a factor of ~ 2.75. Whatever the type of biomass used, it is usually observed that the N contained in the biomass is nearly equally distributed between the aqueous or organic phases, after HTL.[47] In our case 60% of total N was recovered in the biocrude.

3. Rheological properties

As mentioned previously, we have already shown that the hydrophobic fraction resulting from the transformation of *Scenedesmus* sp. residues by HTL at 260 °C had rheological properties similar to a petroleum bitumen. To investigate the potential influence of cerium nitrate on these properties, the complex modulus of both catalytic and non-catalytic hydrophobic HTL fractions was plotted as Black space diagrams (Figure 2). This graphical representation shows the relation between the stiffness |G*| and the phase angle d (°) for all temperature/frequency couples chosen for the measurements. It can be considered as the overall rheological signature of the material. A standard 35/50 petroleum bitumen was plotted as well for comparison.

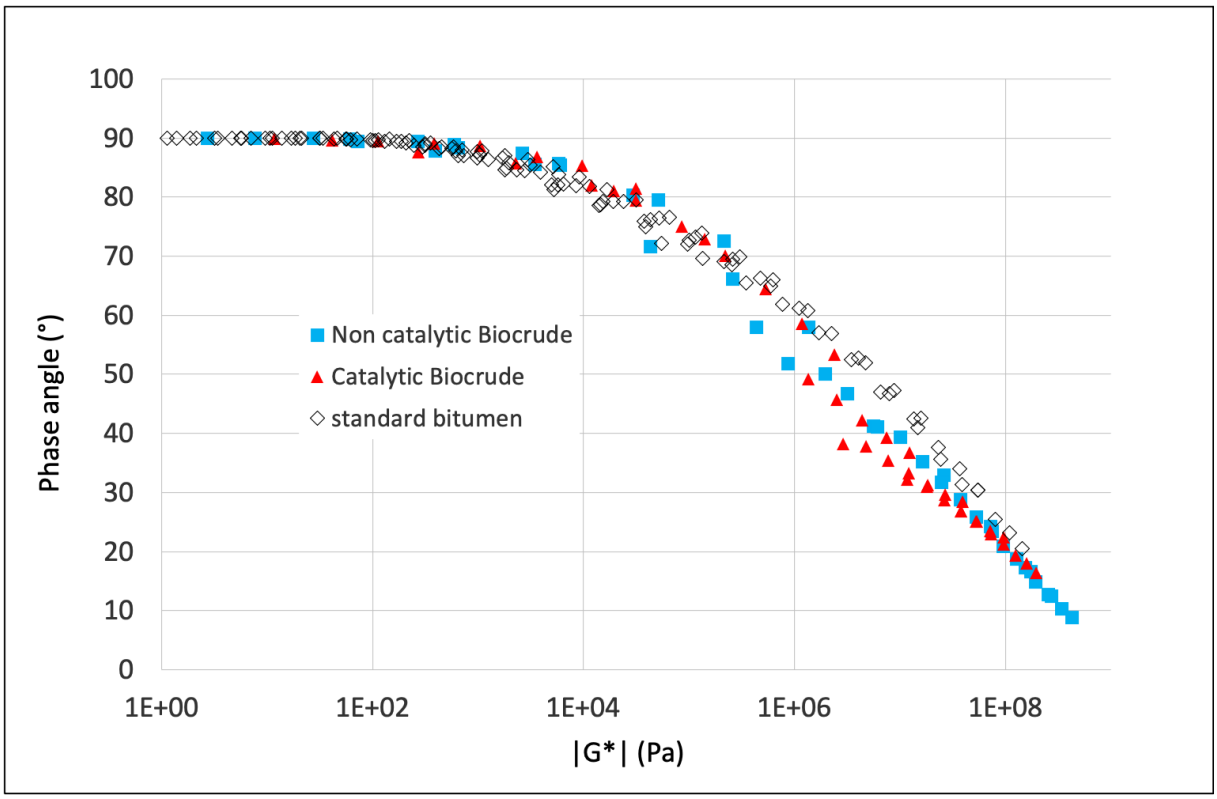


Figure 2. Black diagrams for the hydrophobic HTL fractions (with and without catalyst), by comparison with a standard bitumen.

Figure 2 shows that the overall linear viscoelastic signature for both hydrophobic fractions are similar to that of a petroleum binder. It means that both biocrudes behave like Newtonian

viscous liquid at high temperatures (i.e. phase angle = 90° whatever the frequencies), and like an elastic solid at low temperatures (phase angle reaches 0° in the glassy state). Between these two states, the viscoelastic properties undergo a smooth continuous transition. However, the biocrude prepared in the presence of cerium nitrate presented some isotherm discontinuities in the low temperature domain. This slight destructuration phenomenon with temperature might be due to solid cerium oxide trapped in the material.

The yield for the catalytic biocrude was around 50% with a content of ca. 0.8 wt% of cerium oxide that might increase the rigidity. The stiffness isochrones at 1 Hz as a function of temperature are presented in Figure 3 and the rheological data for a conventional bitumen are given for comparison. Interestingly, the stiffness of the hydrophobic fraction obtained after HTL was higher than the one obtained after catalytic HTL, which in addition showed a transition at 45° where the stiffness suddenly decreased. This suggested that the use of cerium nitrate resulted in a modification the chemical composition of the hydrophobic fraction, leading to a narrower molecular distribution and a more viscous material.

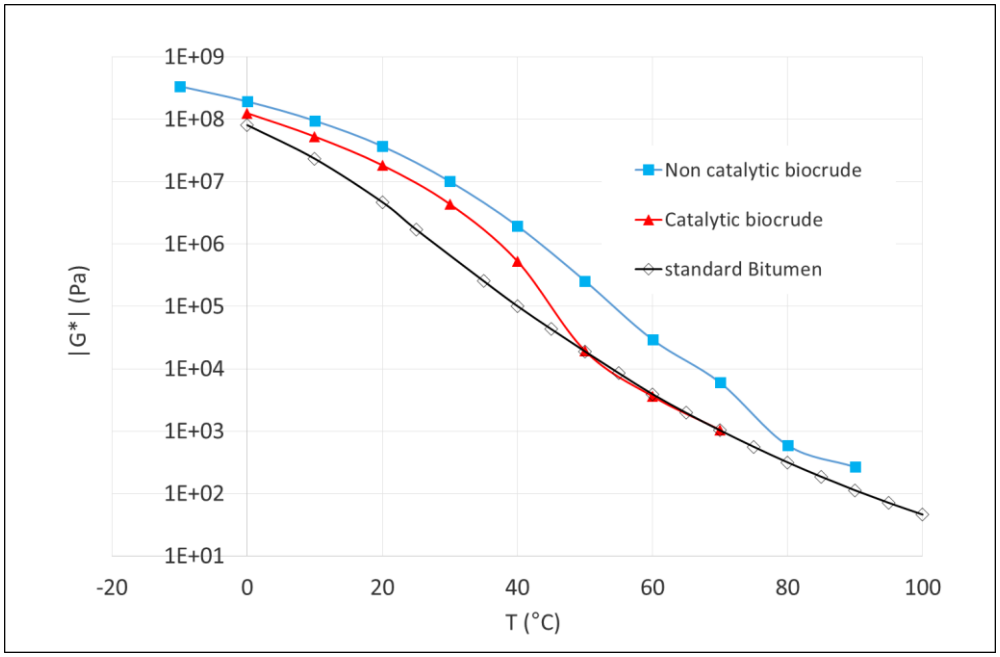


Figure 3. Norm of the complex modulus as a function of temperature (at 1 Hz) for the hydrophobic HTL fractions

We could notice as well that both fractions were stiffer than a standard bitumen, except in the high temperatures domain when a catalyst was used, for which a rigidity similar to that of a standard bitumen was obtained. Those differences are either due to the presence of ceria particles in the hydrophobic fraction (but they represent only 0.8 wt% and normally tend to increase the stiffness, the opposite is observed in our case) or to differences in the chemical composition (increase of the average DBE, vide infra).

3.4. GCxGC and GPC

To characterize the vaporizable fraction (light fraction) of the hydrophobic part, GCxGC-MS analyses were performed. Although the vaporizable fraction represents only a small fraction of the biocrude components, both hydrophobic fractions contained the same families of light compounds: (i) linear and branched long chain alkanes and alkenes; (ii) free fatty acids and their amide derivatives; (iii) nitrogen-containing heterocyclic compounds, including piperazine, pyrrole, pyrrolidine, and morpholine-based derivatives (Figure S1 and S2 in the supporting information).

Gel permeation chromatography (GPC) was also used to investigate the influence of the catalyst on the distribution of molecular masses in the hydrophobic fraction. The molecular weight distribution is presented in Figure 4. For both samples, the same multimodal distribution was observed, however with significantly more heavy compounds in the absence of catalyst (between 700 and 1200 g/mole PS eq.). The two peaks at ca. 500 g/mol PS eq. and 565 g/mol PS eq. might represent fatty acids and sterols. The heaviest part around 760 g/mol PS eq. might correspond to various families of compounds such as peptides derivatives, bounded fatty acids,

heavy alkyl PAHs and condensed nitrogen compounds identified hereafter. Lopez Barreiro et al.[48] proposed a molecular model of biocrude oils obtained from HTL with such families of compounds. In the present paper, particular attention was paid to the characterization of large size N-containing polycyclic compounds.

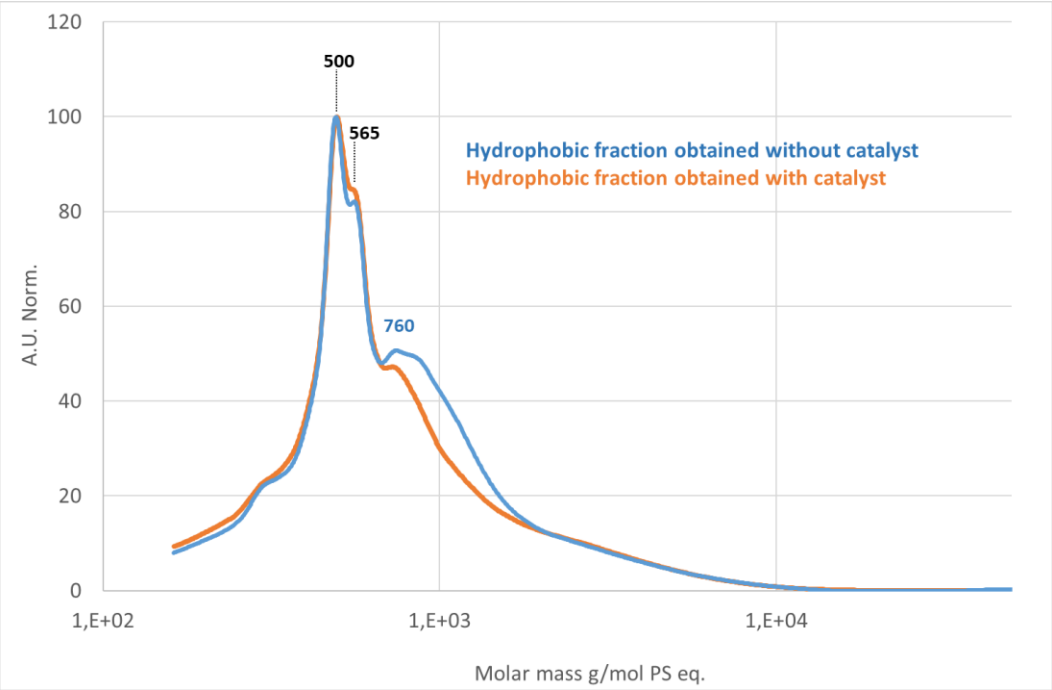


Figure 4. Molecular weight distribution curve measured by GPC, for the hydrophobic fraction: red (with catalyst), blue (no catalyst).

3.5. FT-ICR MS

Fourier transform ion cyclotron resonance mass spectrometry (FT-ICR MS) was then applied to analyze the high molecular weight fraction of both HTL hydrophobic fractions and study the influence of the catalyst during HTL. The positive and negative ion mass spectra obtained by LDI FT-ICR MS analysis exhibited broad and complex distributions of compounds ranging from 180 to 600 m/z. Each LDI final spectrum is the average of 50 spetra, the discrepancy in compounds distribution is a few %.[49] The negative LDI FT-ICR MS of both hydrophobic fractions are presented in Figure S3. The observed average masses are 350 and 382 m/z for catalytic and non-catalytic samples, respectively, for the negative mode and 300 and 309 m/z

for the positive mode. The catalytic sample exhibited a slightly broader mass distribution. The non-catalytic biocrude analysis led to the detection of 847 signals in the positive detection mode and 719 peaks as negative ions. Negative ions were detected either as $M^{\bullet -}$ radicals (~20% of the total ion current) or deprotonated $[M-H]^-$ ions (~80% of the total ion current). Deprotonated features are mainly assigned to "neutral" nitrogen compounds. The protonated ions (~80% of the total ion current) observed in the positive detection mode are mainly related to basic nitrogen compounds. The $M^{\bullet +}$ radical cations (~20% of the total ion current) are mainly relative to aromatic and polyaromatic compounds for which the removal of an electron ensures the extension of the π conjugation domain and the stabilization of the ion.[50]

The chemical formulae assigned to each detected signal revealed similarities between non-catalytic and catalytic biocrudes, whatever the ion detection mode. LDI-FT-ICR MS at 355 nm is known to be very efficient for the ionization of heteroaromatic compounds, in particular N containing molecules. Negative ionization favors the detection of (highly) oxygenated compounds (up to O5, e.g. N5O5) whereas the positive mode favors protonation of small N aromatics.[49,51] Hence the negative mode leads to larger O/C and N/C ratios.[52]

In the case of our experiments, the main detected ions were associated with $C_xH_yN_z$ and $C_xH_yN_zO_w$ species and their distribution is illustrated in Figure 5.

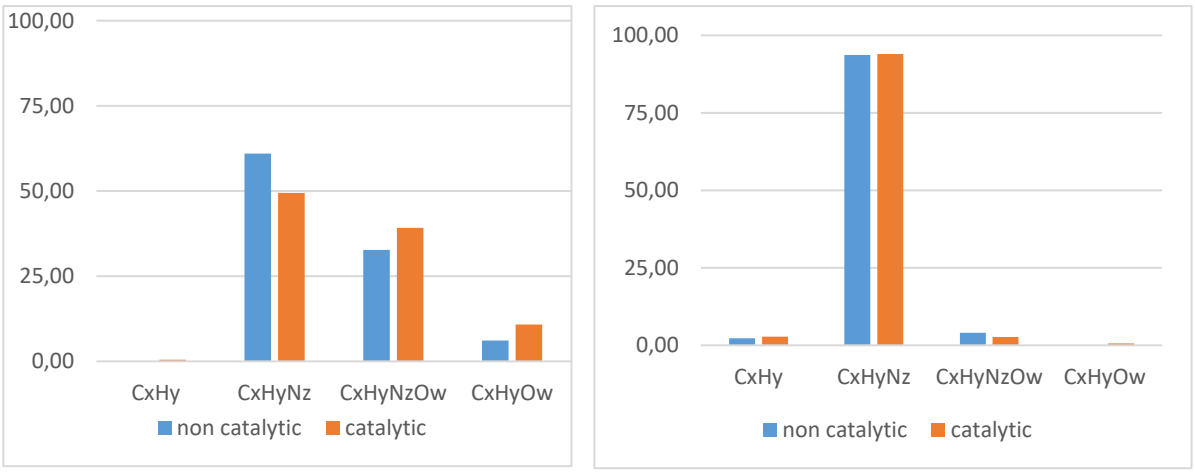


Figure 5. Class distribution obtained for the negative ion mode (left) and the positive ion mode (right) for both radical and non-radical species

Nitrogen containing molecules contributed largely to the heavy part of the hydrophobic fraction due to the remaining proteins (c.a. 25%) in the initial algal residue.

In addition, the number of N (resp. O) heteroatoms was centered around 2 (up to 3, respectively) in the case of a positive ionization (see Figure 6) while this value was centered around 3 (up to 5, respectively) (Figure S4) for a negative ionization.

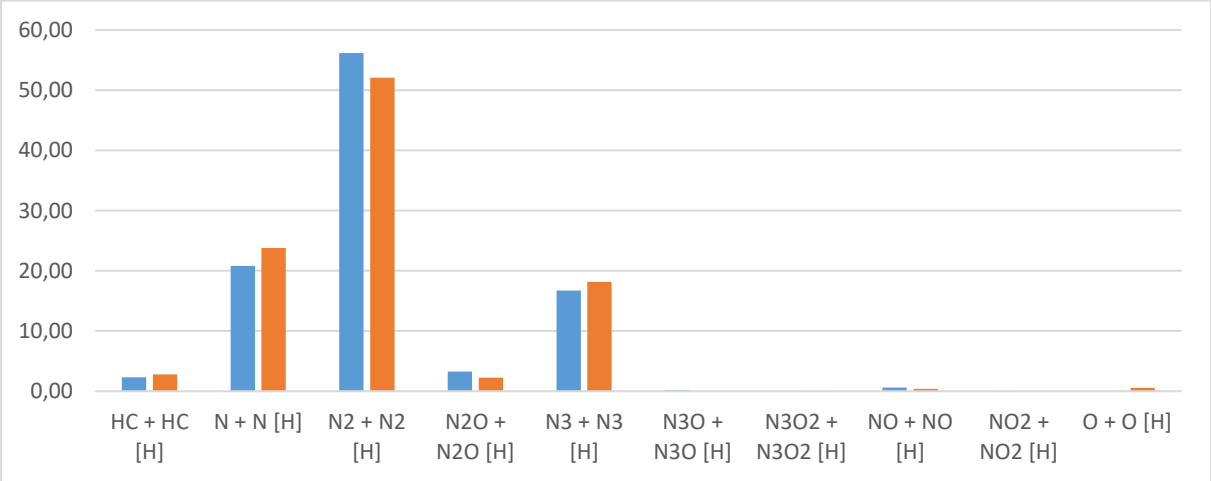


Figure 6. Distribution of radicals and deprotonated compounds (FT-ICR in the positive mode), as a function of their N and O content, for biocrudes obtained in the absence (blue) or presence (orange) of cerium nitrate.

Many studies have reported that biocrudes resulting from the HTL of microalgae contained a high amount of N molecules. For example, this was evidenced by FT-ICR MS in the case of *C. Merolae* and *G sulphuraria*,[53,54] *Nannochloropsis Salina*,[21,54] *C. Vulgaris*[55] or *Chlorella sp*,[56] for which N_2Ox ($0<x<4$) was the most abundant class of compounds. By contrast, in the

case of *Nannochloropsis sp.*, the N_3Ox class was found to be the most abundant,[57] similarly to what we observed when using *Scenedesmus sp.* residues.

The plot of DBE versus carbon number gave evidence of a broad variation of the alkylation and aromatization depending whether cerium nitrate was added or not. When cerium nitrate was used, higher m/z values were observed in the negative mode (see Figure S5 representing the DBE vs carbon number of all the ions whatever the class), resulting in an increase of the average DBE from 19.2 (no catalyst) to 20.5 (with cerium nitrate), the average carbon number being centred near C_{25}. The same trend was also present in the positive mode (average DBE varying from 13.2 to 15.3). Positively ionised molecules tend to be less aromatic than negatively ionised one. The general trend of the distribution is a simultaneous increase of the C content and aromaticity. This type of distribution, although narrower in our case, has already been observed on the biocrude obtained from the HTL of *Nannochloropsis Salina* [21] or *Chlorella sp.*[56] analyzed by ESI FT-ICR-MS.

The H/C versus N/C modified Van Krevelen diagram confirmed the conclusions obtained when considering the plot of DBE versus carbon number (Figure 7), i.e. cerium nitrate enhanced the relative amount of unsaturated compounds, whatever the nature of nitrogen compounds. This was even more pronounced in (+) LDI for compounds with a small nitrogen content (N/C ranging from 0.05 to 0.075), suggesting that such basic nitrogen compounds are more sensitive to the catalyst than the others. In contrast, the increase of unsaturation when a catalyst was used seemed to be poorly dependent of the N/C ratio when considering the (–) LDI van Krevelen diagrams. A global shift of the dot cloud between positive and negative ions to the lowest H/C ratio was observed (especially for the most abundant detected feature).

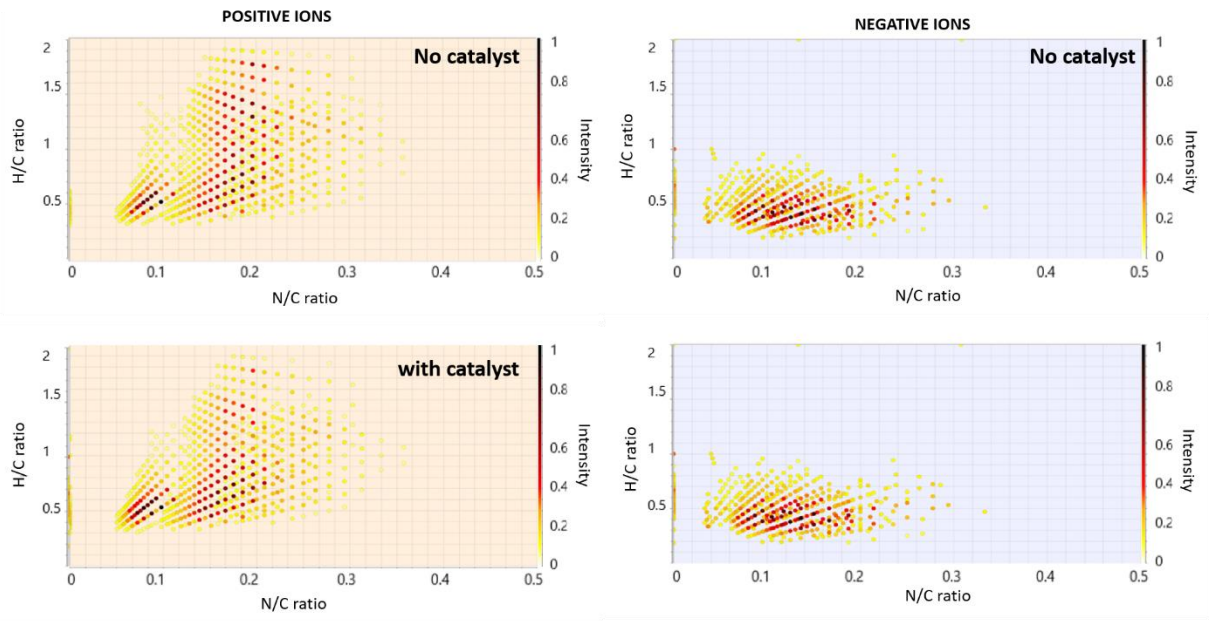


Figure 7. Van Krevelen diagram obtained after positive (left) and negative (right) LDI-FTICR MS for non-catalytic (top) and catalytic (bottom) HTL experiments.

LDI ionisation provides a specific insight on N-containing compounds. For instance, as illustrated by Figure 8, the response of N containing basic compounds (pink) by positive ionisation is much more intense than that of hydrocarbons. They exhibit a wide distribution in terms of H/C ratio and DBE range and the use of cerium nitrate did not influence this compound distribution. We have assumed that conventional DBE expression corresponding to trivalent N atoms could be used in our case, since no particular atomic valences were present in our compounds.[58]

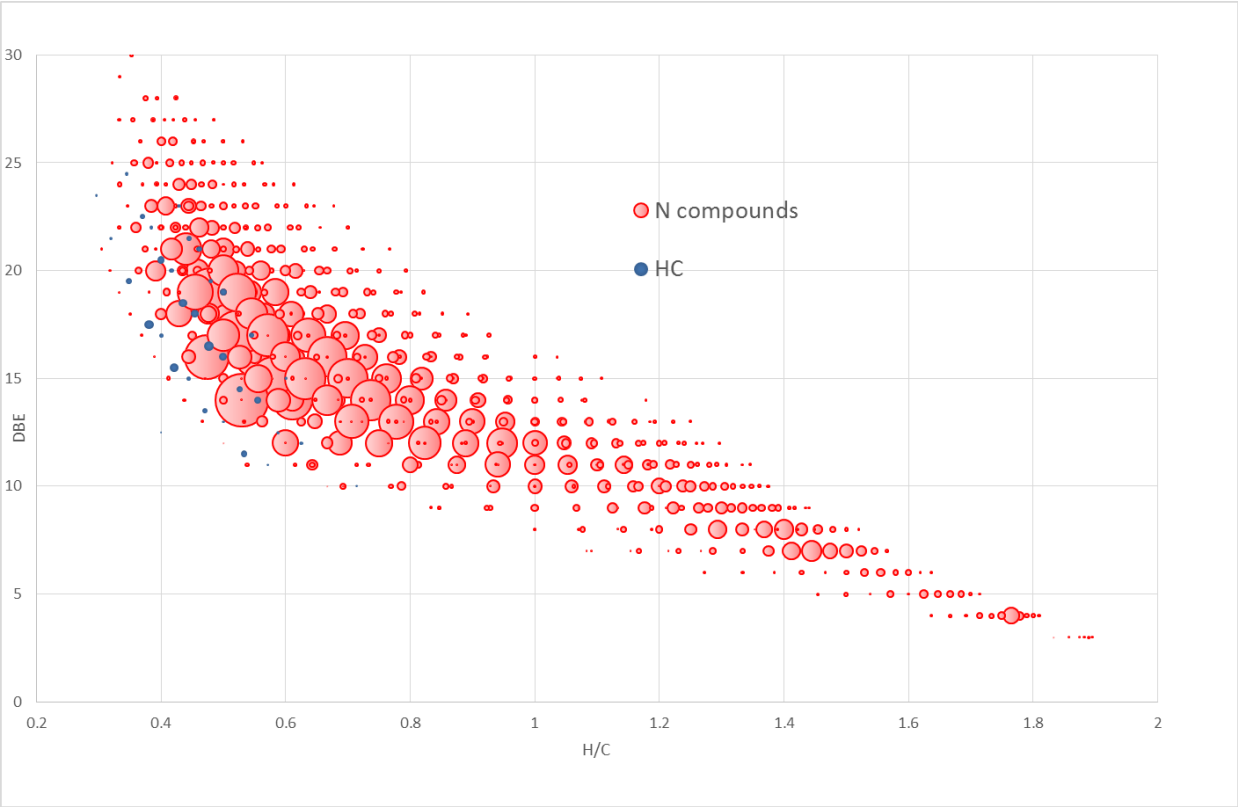


Figure 8. Distribution of DBE versus H/C in positive mode of non-catalytic HTL biocrude.

Another illustration of the abundance of N compounds in the HTL biocrude is shown by the distribution of the main families of basic compounds, namely protonated N1 and N3, in the non-catalytic sample. For the catalytic sample, a few compounds with higher DBE are systematically observed (Figure S6 and S7).

The composition of HTL oils has been investigated by Torri et al.[59] and different families of compounds were identified:

1. Pyrazines: GC detectable products resulting from the Maillard reaction between sugars and amino acids or amines (formed by amino acid decomposition) and pyrolysis products of melanoidin-like polymers.[20]

2. Pyridines: pyrolysis products of “strongly” charred/coked proteins (“black nitrogen”) and pyrolysis products of Melanoidin-like polymers.[20]

3. Pyrroles: pyrrole derivatives (pyrrole and various alkylpyrroles), markers of melanoidin polymers,[21] also produced from the pyrolysis/thermal degradation of chlorophylls(porphyrin) and proteins ("black nitrogen").[22]

4. Alkylnitriles and fatty-amides: HTL products formed by the condensation of ammonia (from proteins pyrolysis) and fatty acids.[23]

5. Indoles, phenols, and aromatic amides: pyrolysis products likely produced from the side chains of aminoacids (such as phenylalanine, tryptophan, and tyrosine).[24]

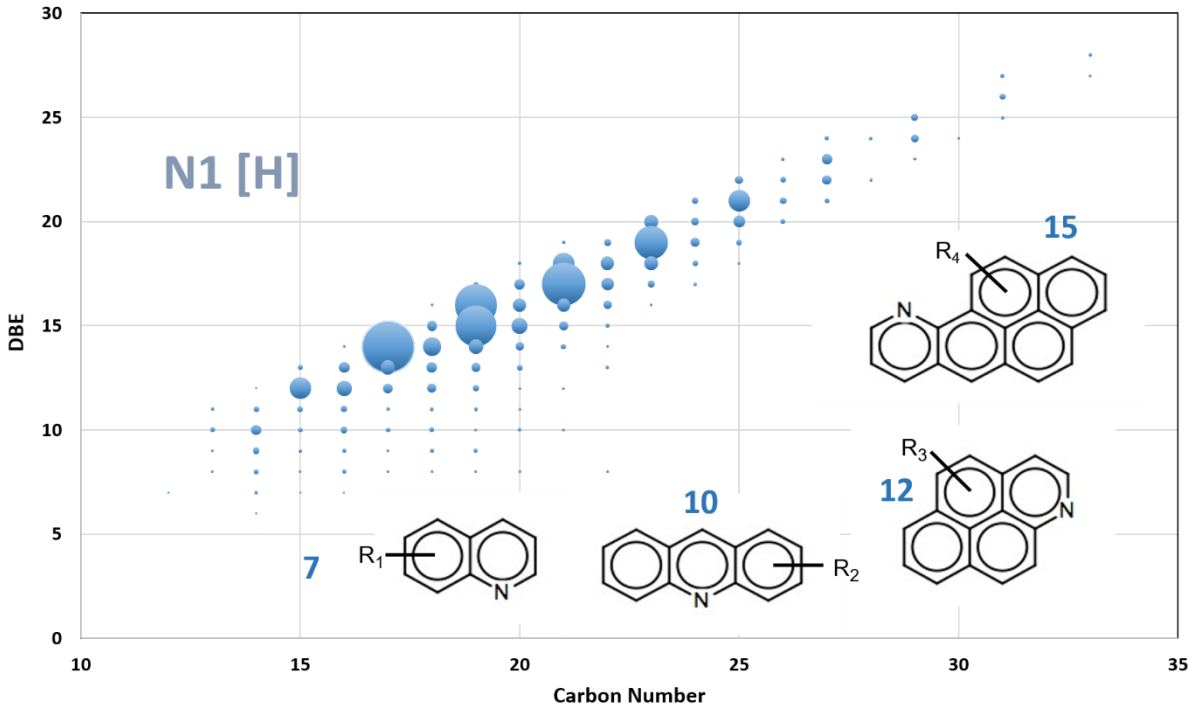
6. Polycyclic aromatic hydrocarbons (PAHs): polycyclic aromatic hydrocarbons with two or more aromatic rings, mainly in polyalkylated form, which can be formed from various biological precursors during the HTL or pyrolysis of the biomass.[25]

Sudasinghe proposed, from the (+) ESI FT-ICR-MS analysis of the HTL biocrude of *Nannochloropsis Salina,* that N1 family is derived from pyridine and quinolone and N2 family is derived from imidazole and pyrazine.[21] Our (+) LDI FT-ICR-MS analyses revealed similar heavy compounds. Indeed, N1 [H] and N2 [H] families were associated to the protonation of basic compounds on a wide range of DBE. For the N1 [H] family (see Figure 9), compounds exhibited DBE from 7 to 29. Some molecular structures can be proposed from the molecular weight and DBE of the analysed fragments. For instance, DBE = 7 could be attributed to quinoline and for DBE 7+ 3x ($1<x<7$) to acridine, tribenzo, tetrabenzo, … quinolines with alkyl chains ranging from C3 to C6. In general, the simultaneous increase of the DBE and the carbon number by two may be considered as the extension of the aromatic domain. Indeed, the number of unsaturation increase by two when an additional aromatic ring is involved (one for the ring and one for the supplementary C2 unit. DBE = 12 and 12+ 3x ($0<R_3<5$) was assigned to azapyrene. We can notice as well a strong contribution of phenalenoindole (DBE = 14) and azabenzopyrene (DBE = 15) and associated compounds occurring from the condensation with

another aromatic ring (Cn of +2) at DBE = 16 and 17 (DBE increment of +2 respectively). These families can lead to higher condensed systems by addition of an aromatic ring (DBE +2 or +3). Finally, the highest DBE of 26 could be represented by an ovalene-like structure (10 aromatic rings) with one nitrogen atom ($C_{31}H_{13}N$, phenanthrochrysenophenanthridine).

N2 [H] was the most abundant family, with DBE ranging from 3 to 29 with the following assignment: DBE = 3 (imidazoles with branched carbons C_7< R5 <C_{14}), DBE = 6 (azaindoles with C_3< R7< C_{14}), DBE = 7 (quinazoline with C_3< R_8 <C_{16}) and DBE = 9 (pyridoindole with C_0 <R9< C_{13}), respectively.

N3 [H] was the most complex one. We did not observe imidazopyridine (DBE = 6), since N3 compounds were in the 7 to 27 DBE range, and three tentative model compounds are given for DBE values of 7, 9 and 11, respectively.



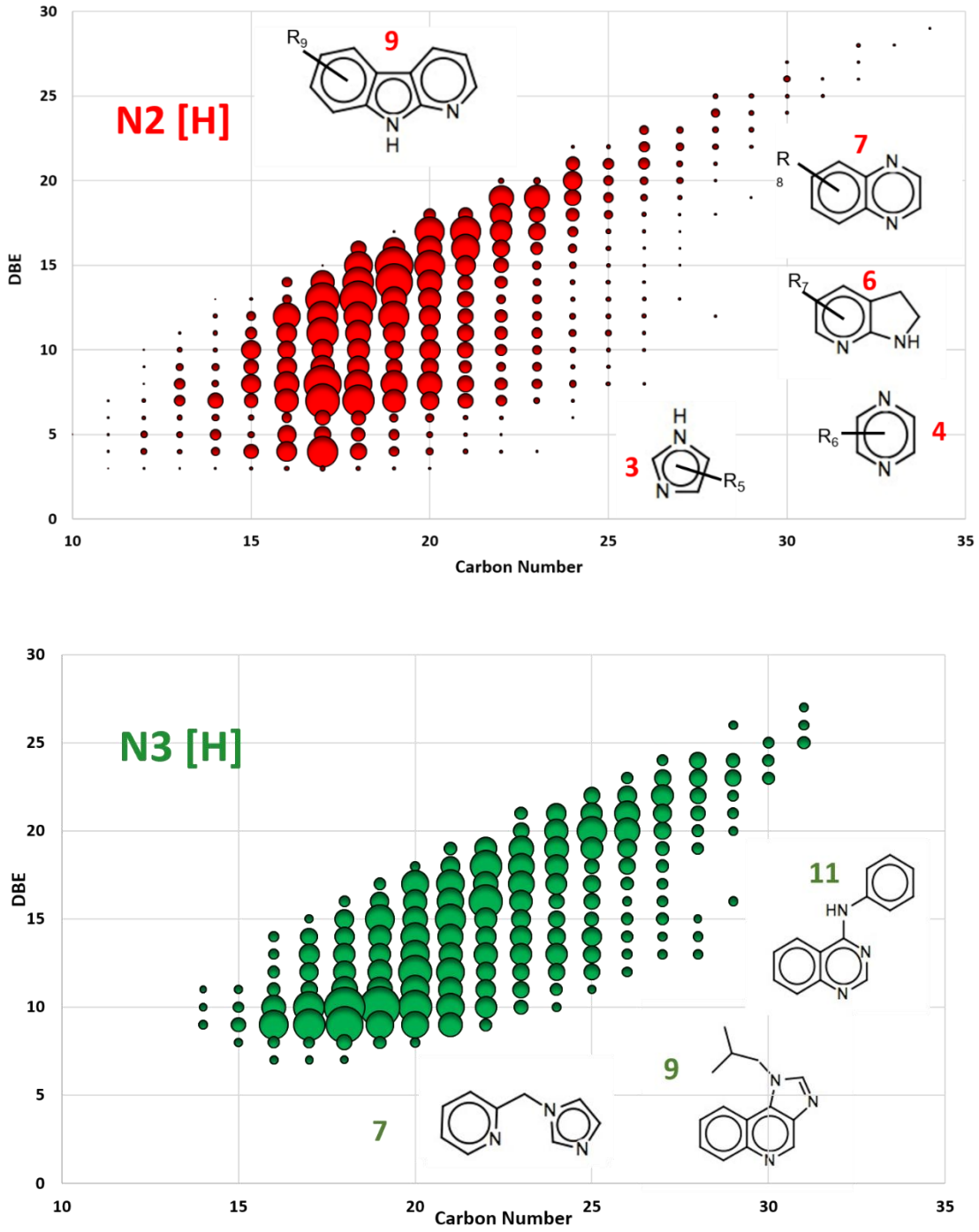


Figure 9. DBE versus carbon number plots of protonated N1, N2, N3 species detected for the positive ionisation mode, for the biocrude obtained after non-catalytic HTL. The structure of some N compounds with their DBE are illustrated for each family.

While the negative mode favours the ionisation of oxygenated compounds and non-basic N compounds, the distribution of DBE versus H/C was found to be narrower than the positive

mode (see Figure 10) and exhibited few long chain compounds (low DBE, H/C=2). From DBE versus carbon number plot of Nx [H] deprotonated compounds (not shown), no DBE below 10 was observed and the number of alkyl chains was limited to C_6.

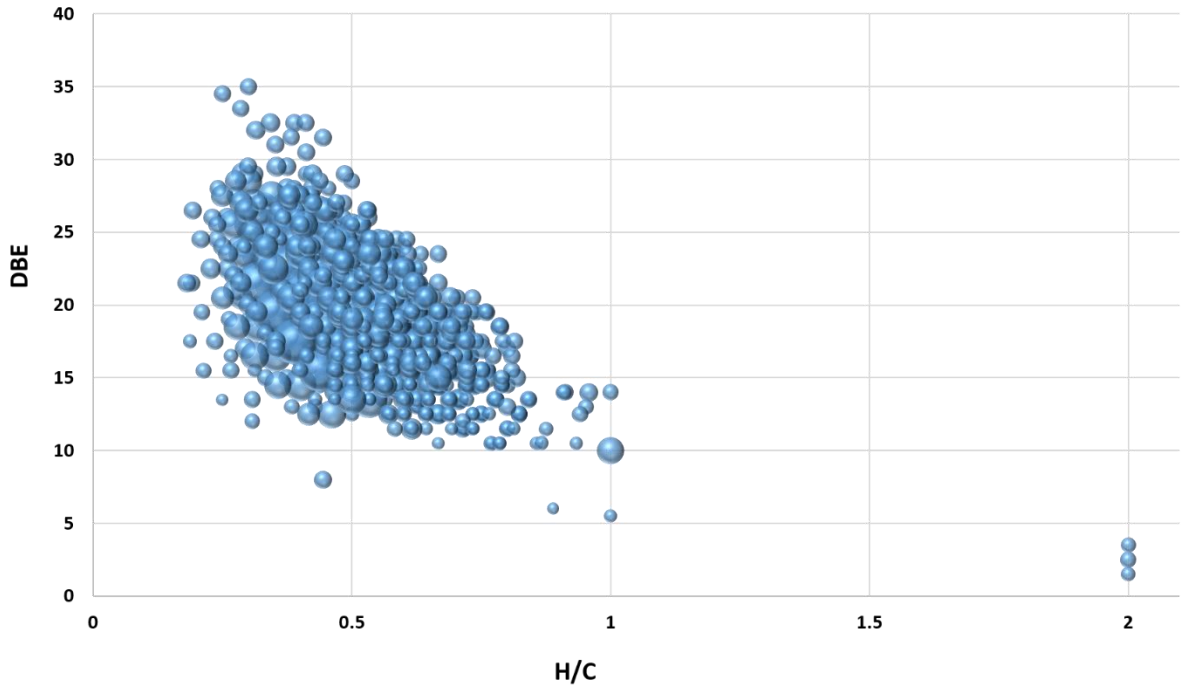


Figure 10. Distribution of DBE versus H/C for Nx and NxOy deprotonated species detected in the negative ionisation mode, for the non-catalytic HTL biocrude.

Figure 11 illustrates the distribution of DBE versus carbon number for the Nx and NxOy families. No diketopiperazine like compounds (DBE= 3) were observed. N_1O_x included pyrrole, indole and carbazole like compounds with oxygenated functional groups, and N2O1 and N2O2 oxygenated alkyl imidazoles and oxygenated alkyl pyrazines, respectively.[21] Among N4 compounds (DBE higher or equal to 15), $C_{20}H_{14}N_4$ (DBE =16) could be assigned to porphyrin. This type of compounds have been observed by Jarvis et al.[60] and found to be refractory to further hydrotreatment. Several related compounds were assumed to be present at higher DBE.

In summary, FTICR-MS demonstrated that heavy N-containing molecules with condensed aromatic ring similar to the asphaltenes found in fossil bitumen are formed in biobitumen obtained from Scenedesmus residues.

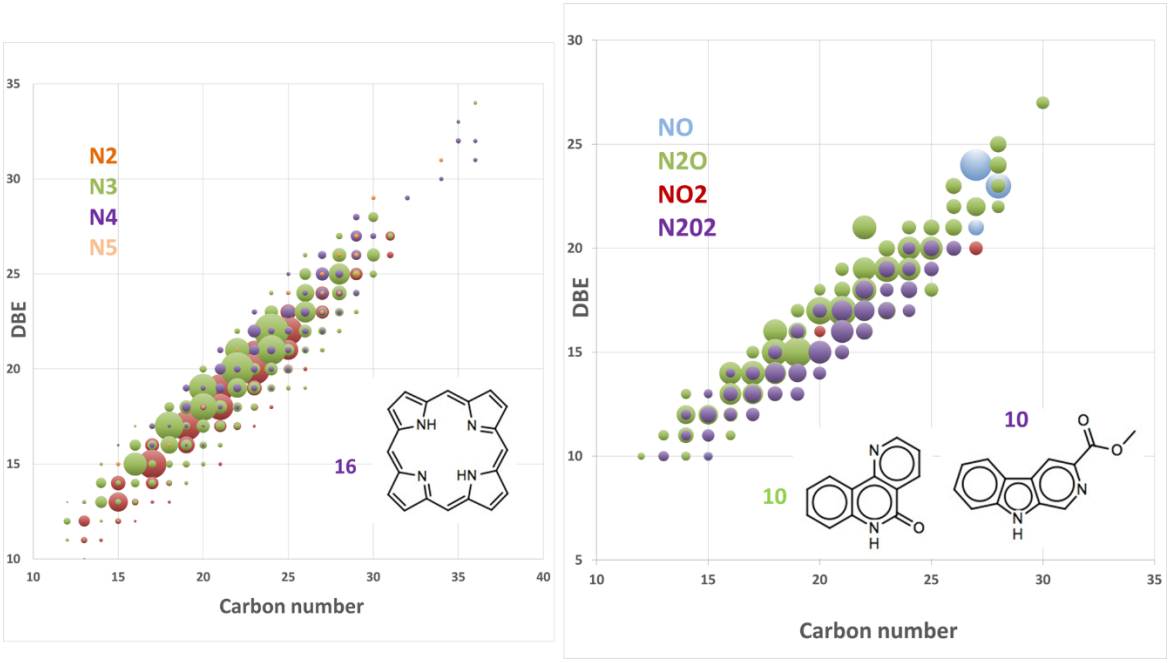


Figure 11. Distribution of DBE with carbon number for Nx and NxOy species detected in the negative ionisation mode for the non-catalytic HTL biocrude, and proposed structures for porphyrins and NxOy compounds.

4. Conclusion

We have shown that byproducts of the microalgae industry could be used to produce biobitumen with a rheological behavior close to that of conventional bitumen. The composition of this biobitumen obtained from HTL with or without cerium nitrate was characterized and a detailed analysis of the molecules of intermediate molecular weight was performed by FT-ICR MS. More than 800 molecules with molecular weights ranging from 165 to 450 were identified in the positive ionization mode and more than 700 (180<Mw< 510) in the negative mode. Thanks to LDI ionization many N-containing molecules were identified, including various families of NxOy compounds either basic or neutral rich in N-containing aromatic rings, as well as

porphyrins. Playing a role similar to asphaltenes in petroleum bitumen, these 'asphaltene-like' compounds with high boiling points, high aromaticity and alkyl chains might contribute to the unique rheological properties of the biobinder obtained by HTL of microalgae residues. When $Ce(NO_3)_3$ is added, the stiffness of the biobinder is closer to the one of petroleum bitumen than in the absence of catalyst, especially in the high temperatures domain.

Acknowledgement

This work received the financial support of the University of Gustave Eiffel (doctoral grant of I. B.), and ANR (Algoroute project, grant ANR-16-CE08-0017). Financial support from the National FT-ICR network (FR 3624 CNRS) for conducting the research is gratefully acknowledged.

Appendix A. Supplementary data

Supplementary material related to this article can be found, in the online version.

References

[1] L. Christenson, R. Sims, *Biotechnology Advances* **2011**, *29*, 686.
[2] M. Kumar, Y. Sun, R. Rathour, A. Pandey, I. S. Thakur, D. C. W. Tsang, *Science of The Total Environment* **2020**, *716*, 137116.
[3] M. Möller, P. Nilges, F. Harnisch, U. Schröder, *ChemSusChem* **2011**, *4*, 566.
[4] Y. Hu, M. Gong, S. Feng, C. (Charles) Xu, A. Bassi, *Renewable and Sustainable Energy Reviews* **2019**, *101*, 476.
[5] M. Audo, M. Paraschiv, C. Queffelec, I. Louvet, J. Hemez, F. Fayon, O. Lepine, J. Legrand, M. Tazerout, E. Chailleux, B. Bujoli, *Acs Sustainable Chemistry & Engineering* **2015**, *3*, 583.
[6] I. Borghol, C. Queffelec, P. Bolle, J. Descamps, C. Lombard, O. Lepine, D. Kucma, C. Lorentz, D. Laurenti, V. Montouillout, E. Chailleux, B. Bujoli, *Green Chem.* **2018**, *20*, 2337.
[7] I. Nava Bravo, S. B. Velásquez-Orta, R. Cuevas-García, I. Monje-Ramírez, A. Harvey, M. T. Orta Ledesma, *Fuel* **2019**, *241*, 255.
[8] S. Koley, M. S. Khadase, T. Mathimani, H. Raheman, N. Mallick, *Energy Conversion and Management* **2018**, *163*, 111.
[9] K. Kohansal, A. Tavasoli, A. Bozorg, *Bioresource Technology* **2019**, *277*, 136.
[10] F. Y. Han, M. Komiyama, Y. Uemura, N. E. Rabat, *The Journal of Supercritical Fluids* **2020**, *157*, 104704.

[11] P. Biller, R. Riley, A. B. Ross, *Bioresour. Technol.* **2011**, *102*, 4841.
[12] A. B. Ross, P. Biller, M. L. Kubacki, H. Li, A. Lea-Langton, J. M. Jones, *Fuel* **2010**, *89*, 2234.
[13] R. Shakya, J. Whelen, S. Adhikari, R. Mahadevan, S. Neupane, *Algal Res.* **2015**, *12*, 80.
[14] M. A. E. Chailleux B. Bujoli, C. Queffélec, J. Legrand, and O. Lépine, *Transportation Research Circular E-C165* **2012**, *Washington*.
[15] Y. Chen, Y. Wu, R. Ding, P. Zhang, J. Liu, M. Yang, P. Zhang, *AICHE J.* **2015**, *61*, 1118.
[16] A. R. Maag, A. D. Paulsen, T. J. Amundsen, P. E. Yelvington, G. A. Tompsett, M. T. Timko, *Energies* **2018**, *11*, 564.
[17] A. G. Marshall, C. L. Hendrickson, G. S. Jackson, *Mass Spectrom. Rev.* **1998**, *17*, 1.
[18] E. N. Nikolaev, Y. I. Kostyukevich, G. N. Vladimirov, *Mass Spectrom. Rev.* **2016**, *35*, 219.
[19] J. M. Jarvis, J. M. Billing, Y. E. Corilo, A. J. Schmidt, R. T. Hallen, T. M. Schaub, *Fuel* **2018**, *216*, 341.
[20] P. Rathsack, M. Kroll, A. Rieger, R. Haseneder, D. Gerlach, J.-U. Repke, M. Otto, *Journal of Analytical and Applied Pyrolysis* **2014**, *107*, 142.
[21] N. Sudasinghe, B. Dungan, P. Lammers, K. Albrecht, D. Elliott, R. Hallen, T. Schaub, *Fuel* **2014**, *119*, 47.
[22] N. Charon, J. Ponthus, D. Espinat, F. Broust, G. Volle, J. Valette, D. Meier, *J. Anal. Appl. Pyrolysis* **2015**, *116*, 18.
[23] N. S. Tessarolo, R. V. S. Silva, G. Vanini, A. Casilli, V. L. Ximenes, F. L. Mendes, A. de R. Pinho, W. Romao, E. V. R. de Castro, C. R. Kaiser, D. A. Azevedo, *J. Anal. Appl. Pyrolysis* **2016**, *117*, 257.
[24] Z. He, M. Guo, R. L. Sleighter, H. Zhang, F. Chanel, P. G. Hatcher, *J. Anal. Appl. Pyrolysis* **2018**, *136*, 96.
[25] I. Leonardis, S. Chiaberge, T. Fiorani, S. Spera, E. Battistel, A. Bosetti, P. Cesti, S. Reale, F. De Angelis, *ChemSusChem* **2013**, *6*, 160.
[26] A. Croce, E. Battistel, S. Chiaberge, S. Spera, F. De Angelis, S. Reale, *ChemSusChem* **2017**, *10*, 171.
[27] R. Olcese, V. Carré, F. Aubriet, A. Dufour, *Energy Fuels* **2013**, *27*, 2135.
[28] R. N. Olcese, G. Lardier, M. Bettahar, J. Ghanbaja, S. Fontana, V. Carré, F. Aubriet, D. Petitjean, A. Dufour, *ChemSusChem* **2013**, *6*, 1490.
[29] J. Hertzog, V. Carré, Y. Le Brech, C. L. Mackay, A. Dufour, O. Mašek, F. Aubriet, *Analytica Chimica Acta* **2017**, *969*, 26.
[30] F. Aubriet, T. Ghislain, J. Hertzog, A. Sonnette, A. Dufour, G. Mauviel, V. Carré, *J. Am. Soc. Mass Spectrom.* **2018**, *29*, 1951.
[31] E. Terrell, V. Carré, A. Dufour, F. Aubriet, Y. Le Brech, M. Garcia-Pérez, *ChemSusChem* **2020**, *n/a*.
[32] O. H. Lowry, N. J. Rosebrough, A. L. Farr, R. J. Randall, *Journal of Biological Chemistry* **1951**, *193*, 265.
[33] E. G. Bligh, W. J. Dyer, *Canadian Journal of Biochemistry and Physiology* **1959**, *37*, 911.
[34] J. Folch, M. Lees, G. H. S. Stanley, *Journal of Biological Chemistry* **1957**, *226*, 497.
[35] M. Dubois, K. A. Gilles, J. K. Hamilton, P. A. Rebers, F. Smith, *Analytical Chemistry* **1956**, *28*, 350.
[36] J. W. T. Blackburn, W. Kew, M. C. Graham, D. Uhrín, *Anal. Chem.* **2017**, *89*, 4382.
[37] J. Hertzog, V. Carré, L. Jia, C. L. Mackay, L. Pinard, A. Dufour, O. Mašek, F. Aubriet, *ACS Sustainable Chem. Eng.* **2018**, *6*, 4717.
[38] J. Hertzog, V. Carré, Y. Le Brech, A. Dufour, F. Aubriet, *Energy Fuels* **2016**, *30*, 5729.
[39] F. Aubriet, V. Carré, In *Fundamentals and Applications of Fourier Transform Mass Spectrometry*, Elsevier, **2019**, pp. 281–322.
[40] S. Mandal, N. Mallick, *Appl Microbiol Biotechnol* **2009**, *84*, 281.

[41] C. A. Gaertner, J. C. Serrano-Ruiz, D. J. Braden, J. A. Dumesic, *Journal of Catalysis* **2009**, *266*, 71.
[42] C. A. Gaertner, J. C. Serrano-Ruiz, D. J. Braden, J. A. Dumesic, *Ind. Eng. Chem. Res.* **2010**, *49*, 6027.
[43] C. A. Gärtner, J. C. Serrano-Ruiz, D. J. Braden, J. A. Dumesic, *ChemSusChem* **2009**, *2*, 1121.
[44] P. SundarRajan, K. P. Gopinath, J. Arun, K. GracePavithra, K. Pavendan, A. AdithyaJoseph, *Renewable Energy* **2020**, *151*, 79.
[45] D. L. Barreiro, S. Riede, U. Hornung, A. Kruse, W. Prins, *Algal Res.* **2015**, *12*, 206.
[46] G. Teri, L. Luo, P. E. Savage, *Energy Fuels* **2014**, *28*, 7501.
[47] L. Leng, W. Zhang, H. Peng, H. Li, S. Jiang, H. Huang, *Chemical Engineering Journal* **2020**, *401*, 126030.
[48] D. López Barreiro, F. J. Martin-Martinez, C. Torri, W. Prins, M. J. Buehler, *Algal Research* **2018**, *35*, 262.
[49] A. Kamissoko, V. Carré, S. Schramm, F. Aubriet, *Rapid Communications in Mass Spectrometry* **2019**, *33*, 95.
[50] M. Lesslie, J. A. Meyer, S. Osburn, S. Otun, V. Ryzhov, *International Journal of Mass Spectrometry* **2015**, *378*, 312.
[51] S. Schramm, V. Carré, J.-L. Scheffler, F. Aubriet, *Atmospheric Environment* **2014**, *92*, 411.
[52] S. Schramm, V. Carré, J.-L. Scheffler, F. Aubriet, *Anal. Chem.* **2011**, *83*, 133.
[53] K. P. R. Dandamudi, T. Muppaneni, N. Sudasinghe, T. Schaub, F. O. Holguin, P. J. Lammers, S. Deng, *Bioresource Technology* **2017**, *236*, 129.
[54] F. Cheng, Z. Cui, L. Chen, J. Jarvis, N. Paz, T. Schaub, N. Nirmalakhandan, C. E. Brewer, *Applied Energy* **2017**, *206*, 278.
[55] J. Zuber, H. Wollmerstädt, T. Kuchling, S. Kureti, P. Rathsack, *Energy Fuels* **2020**, *34*, 3199.
[56] J. M. Jarvis, J. M. Billing, R. T. Hallen, A. J. Schmidt, T. M. Schaub, *Energy Fuels* **2017**, *31*, 2896.
[57] J. L. Faeth, P. E. Savage, J. M. Jarvis, A. M. McKenna, P. E. Savage, *AIChE Journal* **2016**, *62*, 815.
[58] V. V. Lobodin, A. G. Marshall, C. S. Hsu, *Anal. Chem.* **2012**, *84*, 3410.
[59] C. Torri, L. Garcia Alba, C. Samorì, D. Fabbri, D. W. F. (Wim) Brilman, *Energy Fuels* **2012**, *26*, 658.
[60] J. M. Jarvis, N. M. Sudasinghe, K. O. Albrecht, A. J. Schmidt, R. T. Hallen, D. B. Anderson, J. M. Billing, T. M. Schaub, *Fuel* **2016**, *182*, 411.